Stereodynamics of molecular photodissociation

J P Simons

Chemistry Department, The University, Nottingham NG7 2RD, UK

Abstract   The application of tunable, polarised pulsed laser techniques,
in probing molecular photodissociation, is providing unparalleled insight
into their three-dimensional, stereodynamics. A survey of some of the
most recent developments is presented, illustrated by studies of hydrogen
peroxide, t-butyl hydroperoxide, t-butyl nitrite and nitric acid.

INTRODUCTION

When the absorption of a photon by a polyatomic molecule so disturbs its electronic
structure as to promote its fragmentation, it is not surprising that bond-breaking is
accompanied by other structural changes. If the absorption spectrum associated with the
electronic transition is a broad continuum, apart from reflecting a fleeting lifetime for
the electronically excited molecule, and most likely a "half-collisional" direct
dissociation pathway, the spectrum conveys no information on the **dynamics** of the
dissociation process or in particular on its **stereo**dynamics. It is these that convey the
detailed, three-dimensional information relating to the changing geometries of the photo-
excited molecule. The entry into this three-dimensional world is through the door of
'photofragment mapping', i.e. through probing both the scalar (energy) distributions and
the vector (linear and angular momentum) correlations among the recoiling molecular (or
atomic) fragments [1].

Two alternative strategies have been developed to achieve this. The first involves
various methods of photofragment imaging [2,3,4]; the most advanced systems employ laser
ionisation and a multiple detection array to display the angular distribution of the
ionised fragment trajectories [4], while time of flight measurements provide their
velocity/momentum distributions and polarised laser beams provide the essential reference
frame upon which the molecular image can be projected. The second strategy exploits the
polarisation and in particular, the narrow line-width of tunable dye laser systems; the
polarised laser induced fluorescence excitation, or multiple photon ionisation spectra of
the molecular fragments are recorded at sub-Doppler resolution [5-7] in a laser pump
(photolysis)-probe experiment. Analysis of the integrated intensity distributions in the
resolved photofragment spectra provides their energy/quantum state distributions.
Analysis of the Doppler contours of individual spectral lines reveals their velocity
distributions. Finally, and most importantly, analysis of the Doppler contours under
alternative photolysis - probe laser beam polarisation and propagation geometries reveals
the vector correlations (average angles) between the molecular electronic transition
dipole μ_p (referenced to the photolysis beam polarisation ε_p), the fragment recoil
velocity $\mathbf{v}$ and rotational angular momentum $\mathbf{j}$. [8].

In the last few years, these sophisticated new techniques have been used to reveal the
detailed stereodynamics of a range of polyatomic molecules in quite unprecedented detail.
This lecture is designed as an hors d'ouvre which will comprise a discussion of some
exemplary direct photodissociation systems including H_2O_2, $(CH_3)_3COOH$, $(CH_3)_3CONO$ and HNO_3.

VECTOR CORRELATIONS

The correlation between the photofragment recoil velocity $\mathbf{v}$ and the polarisation vector ε_p
of the photolysis beam (and thus the parent molecular transition dipole μ_p) is expressed
by the **translational anisotropy**, $\beta = 2\langle P_2(\mu_p.\mathbf{v})\rangle^{\dagger}$ the first member of an interlocking
triangle of vector pair correlations. The other two, the rotational alignment,

---

† $\langle P_2(\hat{a}.\hat{b})\rangle = \dfrac{3\langle\hat{a}.\hat{b}\rangle^2 - 1}{2}$ where $\hat{a}$ and $\hat{b}$ are unit vectors

$A_0^{(2)} = \frac{4}{5}\langle P_2 (\hat{\boldsymbol{\mu}}_p.\hat{\mathbf{j}})\rangle$ and the $(\mathbf{v}.\mathbf{j})$ correlation, $\langle P_2(\hat{\mathbf{v}}.\hat{\mathbf{j}})\rangle$ both involve the rotational angular momentum of the recoiling fragments. The three correlations can take values lying between the limits

$$2 \geqslant \beta \geqslant -1$$

$$\frac{4}{5} \geqslant A_0^{(2)} \geqslant -\frac{2}{5}$$

$$1 \geqslant (\hat{\mathbf{v}},\hat{\mathbf{j}}) \geqslant -\frac{1}{2}$$

with positive and negative values representing the extremes of parallel or perpendicular alignment. The measured translational anisotropy, β and the rotational alignment $A_0^{(2)}$, can both be 'degraded' by parent molecular rotation either because the dissociation time is long enough to allow significant rotation of the transition dipole $\boldsymbol{\mu}_p$ away from its initial alignment with respect to ε_p, or through the introduction of a tangential (orbital) velocity component. Their interpretation may also be complicated when there is an overlap of two (or more) distinct dissociation continua, with different symmetries, and hence different transition dipolar alignments.

The $(\mathbf{v}.\mathbf{j})$ correlation does not involve the initial transition dipole $\boldsymbol{\mu}_p$; it is an exit channel property, reflecting the dynamics at the instant of fragment separation. None the less, it too may be influenced by the parent molecular rotation, through angular momentum conservation. This may reduce or enhance the effect of vibrational angular motion, e.g. torsion about the breaking bond, which tends to align $\mathbf{j} \parallel \mathbf{v}$ or perpendicular bending motions, which align $\mathbf{j} \perp \mathbf{v}$.

The pair-wise (and higher) correlations between $\varepsilon_p(\boldsymbol{\mu}_p)$, $\mathbf{v}$ and $\mathbf{j}$ are fundamental stereo-dynamical indicators: when they are strong they reflect strong steric influences on the recoiling fragments, from which it is possible to infer the details of the molecular changes which accompany photodissociation. Strong correlations exert a profound influence on both the Doppler profiles and the relative integrated intensities of individually resolved spectral features in the LIF excitation spectra of the recoiling fragments. This occurs because each of the photon absorption steps associated with the molecular photo-dissociation and the fragment LIF probing - are necessarily anisotropic processes. If the photodissociation dynamics generate strongly aligned (or with a circularly polarised photolysis beam, oriented) fragments, their absorption/fluorescence excitation spectra will be strongly polarization dependent [5-10]. The theoretical machinery required to extract the vectorial data from the experimental spectral contours has been developed by Zare [9], Dixon [8], Houston [6] and Docker [11] and will not be discussed here. Although complex it is simple to apply in systems where the fragments recoil with a single, or at least a narrow spread of velocities (e.g. in triatomic molecules and in H_2O). In larger polyatomic molecular photodissociation systems such situations are more likely the exception than the rule, since a broad spread of internal energies in a polyatomic fragment necessarily leads to a corresponding spread of recoil kinetic energies/velocities (through total energy conservation) and a consequent blurring of the recorded Doppler profiles. In practice, however, this has not proved to be a severe problem; the development of Fourier Transform techniques [12,13] for Doppler spectral inversion will further enhance the determination of final energy distributions and hence the precision of the derived vectorial data.

A BENCH-MARK SYSTEM, H_2O_2

In its ground electronic state, HOOH adopts an eclipsed equilibrium geometry, with a dihedral angle ~120°: a small torsional barrier in the trans-planar configuration leads to a splitting of the zero-point vibrational level. U.-v photon absorption is associated with two low-lying electronic transitions, populating the $\tilde{A}^1A$ ($4b(n_0)\to 5b(\sigma_{0-0}^*)$) and $\tilde{B}^1B(5a(n_0) \to 4b(\sigma_{0-0}^*))$ continua. The transitions, not surprisingly, are associated with broad continuum absorption peaking at ~180 nm, but extending a very broad and weak tail towards longer wavelengths. Direct photodissociation can even be effected with blue light (vide infra). Although the $\tilde{A}$ and $\tilde{B}$ continuum states are strongly repulsive along the HO-OH coordinate, their preferred angular geometries are respectively trans ($\tilde{A}^1A$) and cis ($\tilde{B}^1B$) - planar. Polarised laser photodissociation at wavelengths between 248 nm and 308 nm [14-16] generates rapidly recoiling OH fragments which can be detected via LIF spectroscopy. A coaxial pump-probe geometry reveals characteristic 'forward-backward' Doppler spectral profiles, associated with recoil velocities $\mathbf{v}$ directly perpendicular to the transition dipole $\boldsymbol{\mu}_p$. The translational anistropy, β, which lies close to the limiting value $\beta = -1$ (see fig. 1), identifies the principal component in the mid u.-v continuum as ($\tilde{A}^1A \leftarrow \tilde{X}^1A$), with $\boldsymbol{\mu}_p$ lying along the C_2 axis, perpendicular to the O-O bond. At shorter and longer photolysis wavelengths however, the increasing contribution from a centrally peaked, 'sideways' Doppler component, reveals the overlapping $\tilde{B}^1B \leftarrow \tilde{X}^1A$ continuum for which the transition dipole $\boldsymbol{\mu}_p$ lies near parallel to the O-O axis [17]. At
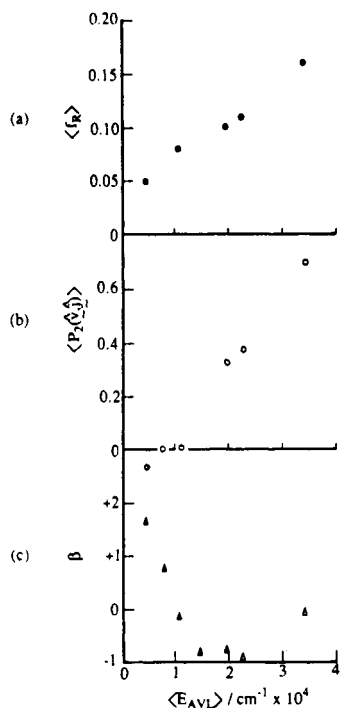
Fig. 1. Absorbed photon energy dependence of rotational energy disposal $\langle f_R \rangle$, the $(\mathbf{v},\mathbf{j})$ correlation and the translational anisotropy β, of OH fragments generated <u>via</u> photodissociation of H_2O_2.

the longest wavelengths, the translational anistropy changes sign and approaches the $\mu_p \| v$ limiting value $\beta = +2$. The narrowing Doppler widths of the recoiling fragments also confirms a single photon photodissociation pathway, even when the energy of the (very weakly) absorbed photon is not too far above the dissociation threshold, see fig. 2.
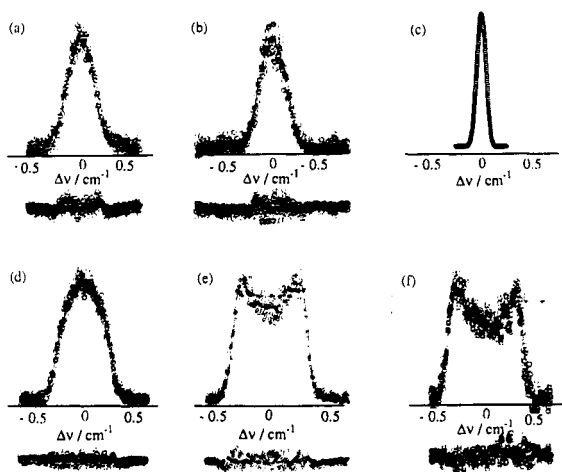
Fig. 2. Doppler resolved profiles of the $R_2(1)$ feature in the A-X LIF spectra of OH fragments, generated <u>via</u> photo-dissociation of H_2O_2 and recorded using coaxial photolysis-probe beam geometry.
(a) 465 nm (b) 455 nm (d) 390 nm
(e) 351 nm (f) 308 nm;
(c) minimum experimental resolution.
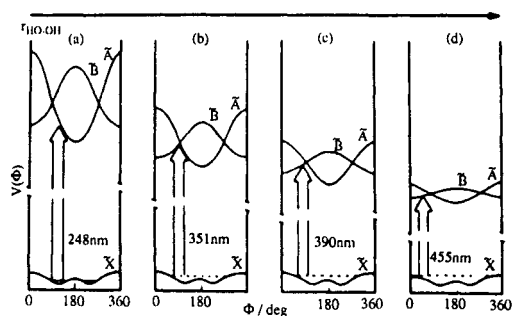
Fig. 3. Schematic sections through the $\tilde{X}$, $\tilde{A}$ and $\tilde{B}$ state potential energy surface of H_2O_2. The vertical arrows indicate the probable shift in the mean torsional angle Φ, of molecules absorbing radiation at wavelengths further and further to the red of the spectral maximum. (Based on data of R. Schinke and V. Staemmler, Chem.Phys.Lett., <u>145</u>, 486 (1988)).

The recoiling fragments carry no detectable energy in vibration, but at short wavelengths particularly, a significant fraction of the available energy, $E_{AVL} \simeq h\nu - D(HO-OH)$, is converted into rotation; this fraction $<f_R>$ decreases almost linearly with decreasing E_{AVL} (see fig. 1). At wavelengths far to the red of the vertical maximum, Franck-Condon considerations restrict photon absorption to the small sub-set of HOOH molecules with greatly extended internuclear HO-OH separations. They will already be well on the way to the dissociation limit in the electronic continuum where the angle bending and torsional anisotropies will be greatly reduced (see fig. 3). The steady decline of $<f_R>$ with decreasing photon energy, implicates angle bending and torsion as the possible engines of fragment rotation. A strong torque associated with motion through a preferred planar geometry (trans <u>via</u> the $\tilde{A}$ state or cis <u>via</u> the $\tilde{B}$ state) would favour torsion and a preferred alignment of the fragment rotation $j \parallel v$, i.e. a 'propeller' motion. This expectation is confirmed by analysis of the Doppler resolved LIF profiles of the rotationally excited OH fragments. Typical profiles, generated by photodissociation at 248 nm, are shown in fig. 4; their high sensitivity to changes in the excitation-detection beam geometries or the polarisation of the related rotational feature (Q-transition aligned parallel to j ; P,R - transition aligned perpendicular to j) betrays a strong positive (v,j) correlation. Quantitative data over a range of photolysis wavelengths are summarised in fig. 1; the decreasing value of the correlation with decreasing energy confirms the decline of torsional anisotropy with increasing HO-OH separation. A simple geometric construction, based on the average values for $(v,j)^2$ and $(\mu_p,j)^2$, determined at 248 nm [14] or 266 nm [16], indicates a trans-planar configuration as the preferred transition state geometry, again as expected for excitation into the $\tilde{A}^1 A$ continuum state.

t-BUTYL HYDROPEROXIDE

In t-butyl hydroperoxide, the introduction of the heavy t-butyl group should introduce two major changes

(a)   The greatly increased mass of the <u>tert</u>-butoxy group will exert a powerful kinematic influence on the OH recoil trajectories.
(b)   The many additional degrees of freedom will introduce a 'sponginess' in the skeletal framework and a considerable change in the partitioning of excess energy between internal and kinetic energy in the separating fragments.
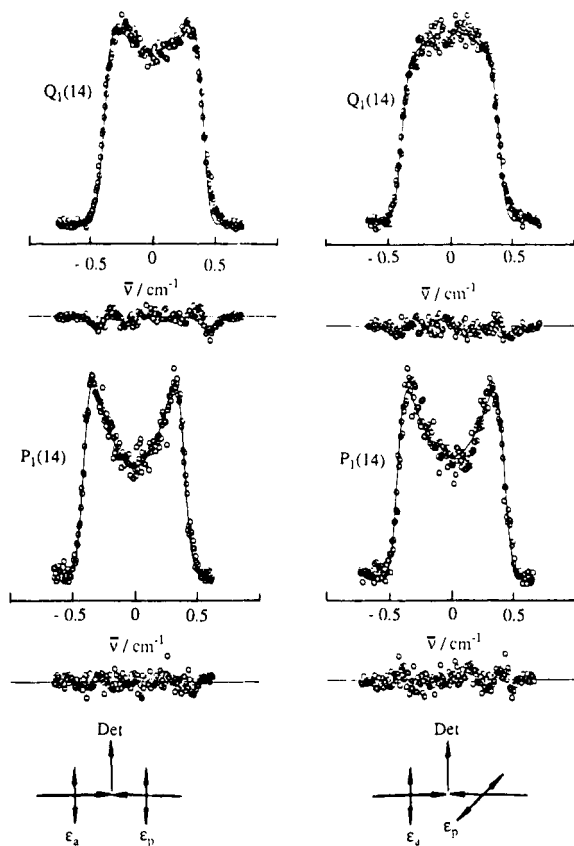
Fig. 4. Doppler resolved profiles of $P_1(14)$ and $Q_1(14)$ features in the A-X LIF spectra of OH fragments, generated <u>via</u> photodissociation of H_2O_2 at 248 nm, using alternative photolysis-probe beam geometries.

Sub-Doppler probing of the LIF spectroscopy of the recoiling OH fragments has quantitatively confirmed both of these expectations [18].

The u.-v. continuum absorption of t-butyl hydroperoxide is little changed from that of H_2O_2 and the retention of its $n_0 \rightarrow \sigma^*_{0-0}$ character can safely be assumed; thus photolysis in the mid u.-v. at 248 nm, by analogy with H_2O_2, might be expected to generate OH fragments, recoiling with translational anisotropies, $\beta \sim -1$. Although still negative, the anisotropy is actually found to be much reduced, with an average value $\beta \simeq -0.3$ [18]. (see table 1). The clue to understanding this change is found in the behaviour of the (v,j) correlation which is also greatly reduced relative to that in H_2O_2 and even changes sign in the lower rotational levels of the OH fragments. Although torsion about the O-O bond still plays a role in promoting the fragment rotation, there is an increase in the relative contribution made by 'perpendicular' OOH, angle bending torques. Their influence is also reflected in the increased rotational alignment $A_0^{(2)}$ (see table 1). An increase in the relative importance of bending as opposed to torsional torques, suggests an initial equilibrium geometry much closer to trans-planar - indeed 'ab initio' calculations for the related alkyl peroxide CH_3OOH, predict a much reduced torsional barrier about the O-O bond [19]. Bending about the OOH angle transfers perpendicular rotational angular momentum to

TABLE 1   Mean vector correlations in OH fragments generated through photodissociation of t-butyl hydroperoxide at 248 nm

Rotational level N	Transational anisotropy β	Rotational alignment $A_0^{(2)}$	(v,j) correlation
4	-0.31	+0.16	-0.15
10	-0.27	+0.14	+0.15
10 †	-0.86 †	+0.10 †	+0.35 †

† comparative data for H_2O_2 [14]

the OH fragment; on the other hand, because of the inertia of the heavy t-butyl group bending about the complementary $(CH_3)_3COO$ bond angle during dissociation will propel the recoiling OH fragment through a spiral trajectory. The resulting 'sling-shot' dynamics rotates the final recoil velocity v away from its initial perpendicular alignment with respect to the parent molecular transition dipole, μ_p; hence $\beta \simeq -0.3$ rather than -1.

The 'sponginess' of the t-butoxy group is revealed by the 'blurring' of the OH Doppler profiles and the reduced kinetic energy release. The reduction reflects the absorption of around one third of the available energy into ro-vibrational motion in the t-butoxy fragment, while the 'blurring' reflects the broad spread of internal energies around the mean value. The energy partitioning is in good agreement with the predictions of a simple impulsive model, consistent with the assumed direct dissociation mechanics. The average internal excitation in the t-butoxy fragments is more than sufficient to promote their unimolecular decomposition

$$(CH_3)_3CO \rightarrow CH_3 + (CH_3)_2CO, \Delta E_0 \simeq + 50 \text{ kJ mol}^{-1} \qquad (1)$$
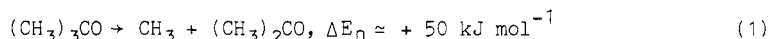
t-BUTYL NITRITE

The equilibrium geometry of t-butyl nitrite is predicted to be trans-planar [20]. Its u.-v absorption has been assigned to two distinct $n_0 \rightarrow \pi^*$ electronic transitions: the first, $\tilde{A}^1A'' \leftarrow \tilde{X}^1A'$ originating on the terminal O atom is associated with a diffuse banded spectrum, while the second, $\tilde{B}^1A' \leftarrow \tilde{X}^1A'$ originates on the central O atom, and generates a structureless continuum. It is this continuum which is accessed by photon absorption at 248 nm. If the trans-planar symmetry is retained during the photodissociation

$$(CH_3)_3CONO + h\nu (248 \text{ nm}) \rightarrow (CH_3)_3CO + NO(X^2\Pi) \qquad (2)$$
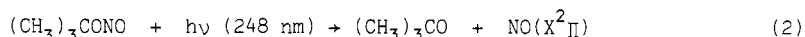
which follows photon absorption, the following stereodynamical features might be anticipated:-

(a)   alignment of the molecular transition dipole μ_p in the molecular plane
(b)   strong rotation of the NO fragment promoted by an impulsive transfer into angular momentum about its centre of mass, and hence directed perpendicular to μ_p.
(c)   a consequent rotational alignment $A_0^{(2)} \rightarrow -0.4$, and (v,j) correlation $\rightarrow -0.5$.
(d)   a translational anisotropy β anywhere between the two extremes $2 \geqslant \beta \geqslant -1$, dependent on the alignment of μ_p relative to the RO-NO bond.

TABLE 2   Mean vector correlations in $(NO)_{v=1}$ "fragments" generated through photodissociation of t-butyl nitrite in the $\tilde{B}^1A' \leftarrow \tilde{X}^1A'$ continuum at 248 nm

Rotational level N	Translational anisotropy β	Rotational alignment $A_0^{(2)}$	$(\mathbf{v},\mathbf{j})$ correlation
51	+1.06	−0.30	−0.51

Table 2 shows the experimental values for each of the vector correlations determined for rotationally excited NO "fragments" in levels j = 40-60 and carrying one quantum of vibrational excitation [18]. As expected, the recoiling NO is almost perfectly aligned perpendicular to the molecular plane and to the recoil velocity: no significant dynamical contribution from out-of-plane torsional motion is apparent. The translational anisotropy is strongly positive and μ_p must be aligned close to the axis of the central O-NO bond.

As with t-butyl hydroperoxide, the pattern of energy disposal lies close to an 'impulsive' expectation, and once again the t-butoxy group absorbs a high fraction of the available energy - this time approaching 50% - and more than sufficient to promote the unimolecular decomposition (1).

HONO₂

Nitric acid is a planar molecule in its ground electronic state. Its u.-v absorption spectrum is entirely continuous displaying a weak, broad maximum centred around 270 nm and a much stronger peak at ~185 nm. Ab initio calculations [21] predict three successive low-lying electronic transitions populating two states of A'' symmetry, populated via $n_{O_2} \rightarrow \pi^*$ transitions. All three excited states are predicted to be non-planar. Photon absorption at any wavelength in the continuum leads to the dissociation(s)

$$HONO_2 + h\nu \rightarrow OH(X^2\Pi) + NO_2(\tilde{X}^2A_1, \tilde{A}^2B_2) \qquad (3)$$
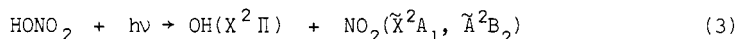
Doppler resolved LIF spectral profiles of the recoiling, rotationally excited OH fragments, generated at 280 nm near the long wavelength peak, and recorded using two alternative excitation-detection geometries, are shown in fig. 5 [22]. The appearance of the 'tell-tale', forward-backward Doppler shape for the perpendicular (fig. 5 (a)), rather than the co-axial geometry, reflects a tendency for recoil in directions parallel to the molecular transition dipole μ_p and suggests that μ_p lies closely parallel to the N-OH bond.

Detailed analysis of the Doppler profiles gives a value for the translational anisotropy, β ≈ +0.8 however, less than the limiting value β = +2. A spiral trajectory, resulting from a planar → pyramidal geometry change in the excited state, and a mean out-of-plane angle of 40°, readily accommodates the difference. Ab initio calculation predicts an out-of-plane angle of 31° [21]. If the stereodynamics had remained coplanar and in the absence of any torsional torque about the breaking N-OH bond, the fragment rotational angular momentum j would have been directed perpendicular both to μ_p and to the recoil velocity v, and the rotational alignment and $(\mathbf{v},\mathbf{j})$ correlations would both have been negative. In practice, both are positive (see table 3)! There is a broad tendency for $\mu_p \parallel \mathbf{v} \parallel \mathbf{j}$.
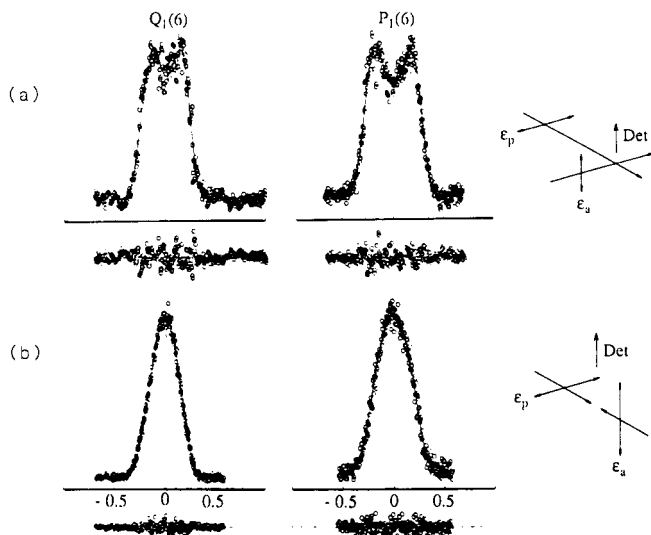
Fig. 5.   Doppler resolved profiles $P_1(N)$, $Q_1(N)$ features in the A-X LIF spectra of OH fragments, generated via photodissociation of HNO₃ at 280 nm, using alternative photolysis-probe beam geometries.

TABLE 3   Mean vector correlations in $(OH)_{v=0}$ fragments generated through photodissociation of HNO at 280 nm [22] and 225 nm [23]

	Rotational level N	Translational anisotropy β	Rotational alignment $A_0^{(2)}$	$(\mathbf{v},\mathbf{j})$ correlation
280 nm	6	+0.88	+0.14	+0.29
	8	+0.8	+0.17	+0.52
225 nm	10	+0.17	+0.08	+0.24

The detailed values of the three stereodynamical indicators can be understood if

(a) the ONO_2 framework of the photoexcited $HONO_2$ becomes pyramidal, and the terminal O-H group becomes twisted out of the initial plane, and
(b) the excited state has A' symmetry.

'Ab initio' calculations [21] (conducted <u>after</u> the experiments!) confirm (a) but predict A'' electronic symmetry for the excited molecule. However, the transition is extremely weak, with an oscillator strength, $f \approx 2 \times 10^{-6}$; a **vibronic** transition involving out-of-plane deformation reconciles experiment with theory.

Stereodynamical studies have also been made for $HONO_2$ molecules excited at 225 nm [23], close to the predicted wavelength for the vertical transition $\tilde{B}^1A'' \leftarrow \tilde{X}^1A'$ [21]. The predicted polarisation of the transition dipole perpendicular to the initial molecular plane, favours a negative value for the translational anisotropy, β, but once again the generation of a spiral recoil trajectory following the planar $\rightarrow$ pyramidal geometry change reduces β from its limiting value: indeed it actually changes sign, to give $\beta \approx +0.2$, corresponding once again, to a mean out-of-plane angle of 40°, cf. the predicted deformation through 31° [21]. Finally the (modestly) positive value found for the $(\mathbf{v},\mathbf{j})$ correlation, reveals the (predicted) torsion about the N-OH bond.

The partitioning of energy beween kinetic and internal motions is profoundly influenced by the strong antibonding character of the π^* m.o. The equilibrium N-O bond lengths in the NO_2 group are predicted to increase by 80-100 pm in the two n $\rightarrow$ π^* states. Since the bond lengths in free NO_2, are virtually the same as those in the ground state of $HONO_2$, simple Franck-Condon considerations predict high vibrational excitation in the NO_2 product. Not surprisingly, detailed analysis of the Doppler profiles, establishes the concentration of around two thirds of the available energy into internal excitation of the NO_2, both at 280 nm ($\tilde{A}^1A''$) and 225 nm ($\tilde{B}^1A''$) [22,23]. Fluorescence from electronically excited NO_2 has also been detected following photodissociation at 241 nm [24].

CONCLUSION

The use of polarised, Doppler resolved laser probing of molecular photodissociation products to expose both their scalar and vectorial properties, has now become a well-established stereo-dynamic strategy. New developments include the measurement of rotational alignment of dissociating systems in real time, using ultra-fast pulsed laser systems [25]; the probing of oriented (unidirectional) systems [26] and oriented fragments [27]; the development of Fourier Transform inversion methods for Doppler profile analysis [12,13] to better cope with the common situation of broadly distributed energy disposals; and the use of three-dimensional photofragment mapping strategies to probe intramolecular vibrational/rotational energy redistribution [28].

Acknowledgements

REFERENCES

1. "Molecular Photodissociation Dynamics", Adv. in Gas Phase Photochemistry and Kinetics,
    Ed. M.N.R. Ashfold and J.E. Baggott, Roy.Soc.Chem., 1987.
2. K.R. Wilson in "Excited State Chemistry", ed. J.N. Pitts, Gordon and Breach, New York,
    1970.
3. A.M. Wodtke and Y.T. Lee, ref. (1), p.31
4. D.W. Chandler and P.L. Houston, J.Chem.Phys. 87, 1445 (1987).
5. J.P. Simons, J.Phys.Chem. 91, 5378 (1987).
6. P.L. Houston, J.Phys.Chem. 91, 5388 (1987).
7. G.E. Hall and P.L. Houston, Ann.Rev.Phys.Chem. 40, 375 (1989).
8. R.N. Dixon, J.Chem.Phys. 85, 1866 (1986).
9. A.C. Kummel, G.O. Sitz and R.N. Zare, J.Chem.Phys. 88, 7357 (1988).
10. D.A. Case, G R McClelland and D.R. Herschbach, Mol.Phys. 35, 341 (1978).
11. M.P. Docker, Chem.Phys. 135, 405 (1989); Chem. Phys. 125, 185 (1988).
12. A. Ticktin and J.R. Huber, Chem.Phys.Lett. 156, 372 (1989).
13. P. Enriques, R. Sayos and J.P. Simons, unpublished work.
14. (a) M.P. Docker, A. Hodgson and J.P. Simons, Faraday Discussions Chem. Soc. 82, 25
        (1986).
    (b) J. August, M. Brouard, M.P. Docker, A. Hodgson, C.J. Milne and J.P. Simons,
        Ber.Bunsenges.Phys.Chem. 92, 264 (1988).
15. K.-H. Gericke, S. Klee, F.J. Comes and R.N. Dixon, J.Chem.Phys. 85, 4463 (1986)
16. M. Brouard, M.T. Martinez, C.J. Milne, J.P. Simons and J.-X. Wang, Chem.Phys.Lett.
    165, 423 (1990).
17. C. Chevaldonnet, H. Cardy and A. Dargelos, Chem.Phys. 102, 55 (1986)
18. J. August, M. Brouard, M.P. Docker, C.J. Milne, J.P. Simons, R. Lavi, S. Rosenwaks and
    D. Schwartz-Lavi, J.Phys.Chem. 92, 5485 (1988).
19. R.A. Bair and W.A. Goddard III, J.Amer.Chem.Soc. 104, 2719 (1982).
20. P. Tarte, J.Chem.Phys. 20, 1570 (1952).
21. Y.Y. Bai and G.A. Segal, J.Chem.Phys. in press.
22. J. August, M. Brouard and J.P. Simons, J.Chem.Soc.Faraday 2 84, 587 (1988).
23. M. Brouard, M.T. Martinez and J.P. Simons, unpublished work.
24. A. Sinha, R.L. Vander Wal and F.F. Crim, J.Chem.Phys. 91, 2929 (1989).
25. A.H. Zewail, J.Chem.Soc.Faraday 2 85, 1221 (1989).
26. R.B. Bernstein, S.E. Choi and S. Stolte, J.Chem.Soc.Faraday 2 85, 1097 (1989)
27. E. Hasselbrink, J.R. Waldeck and R.N. Zare, Chem.Phys. 125, 191 (1988);
    J.Chem.Soc.Faraday 2 85, 1044 (1989).
28. M. Brouard, M.T. Martinez, J. O'Mahony and J.P. Simons, J.Chem.Soc.Faraday 2 85, 1207
    (1989); Mol.Phys. 69, 65 (1990); Phil.Trans.Roy.Soc. in press, (1990).